Journal of Atomic, Molecular, Condensate & Nano Physics
Vol. 3, No. 2, pp. 61–71, 2016
ISSN 2349-2716 (online); 2349-6088 (print)
Published by RGN Publications

http://www.rgnpublications.com

Structural and Optical Studies of Ho^{3+}/yb^{3+} Co-Doped TiO_2 Nanoparticles in Silica Glass

Research Article

S. Rai

Department of Physics, Mizoram University, Aizawl 796004, India
srai.rai677@gmail.com

Abstract. The TiO_2 nanoparticles doped with Ho^{3+} and Yb^{3+} ions were synthesized by sol gel method. The structure of the samples were characterized by XRD, TEM and by thermo gravimetric analysis. The average particle size of the TiO_2 range from 7-10 nm (in diameter). The result obtained from TEM, XRD studies indicate that the rare earth ions were positioned in low phonon glass. The photoluminescence (PL) and upconversion (UC) properties of Ho^{3+} in various concentrations of TiO_2 nanoparticles have been investigated. The PL and UC luminescence depends on particle size and crystal structure and we also observed that the emission of Ho^{3+} in silica xerogel was significantly depends on the amount of TiO_2 nanoparticles.

Keywords. Up conversion; Radiative; Quantum efficiency; TiO_2 nanoparticles; Photoluminescence

PACS. 78.66Jg

Received: February 13, 2015 **Accepted:** December 30, 2015

1. Introduction

Luminescent properties of rare-earth embedded in several metal and semiconductor (SC) nanoparticles (NPs) are used because of their many technological applications. Recently, rare earth (RE) ions doped semiconductor nanoparticles have attracted extensive attention due to their unique optical properties and perspective applications in optoelectronics devices and flat panel displays [1–4]. The luminescence property of RE ions in nanocrystals depends critically on their locations in the host. Since the f-orbital is strongly shielded from the outside ligand, the

positions of the spectral lines vary only slightly with the environment. However, their intensities are strongly dependent on the host in which the RE ion is embedded [5]. In general, the RE emission in glassy matrix is strongly dependent on crystal field's effects, local environment, phonon energy and refractive index where the ion is situated [6]. Silicate glasses which are the most chemically and mechanically stable and also more easily fabricated into various shapes and size. The strong luminescence properties can be realized in the glasses with lower phonon energies. So it is difficult to observe in silicate glasses which posses higher phonon energies. Therefore design of SCNPs doped silica glasses are target at present. Preparing nanoscale host materials can change the physical properties of the host which affects the luminescence and dynamics of optically active dopants. High quality nanocrystalline TiO_2 nanoparticles glass of anatase phase were prepared by using sol-gel techniques. Among the RE ions, Ho^{3+} has been recognized as one of the most efficient RE ions for obtaining laser emission due to its numerous radiative emissions in the visible and IR region. Ho^{3+} ions has been extensively studied in various tellurite glasses and ceramics [7,8] Several transitions are of special interest, the $^5I_7 \rightarrow {}^5I_8$ emission near 2 μm is of particular interest because of its use in eye safe systems and medical applications. The blue, green and red up conversion transitions are very important for lighting applications.

In this work, we report the preparation of silica xerogel doped with Ho^{3+} ions and TiO_2 nanoparticles by sol gel techniques. Structural and luminescent properties of Ho^{3+} codoped with Yb^{3+} in TiO_2-SiO_2 nanoparticles were investigated.

2. Experimental

2.1 Preparation of Er^{3+}/yb^{3+} ions Doped Titania Samples

A facile sol-gel method was introduced to prepare titania (TiO_2) nanoparticles [6]. The titania sol prepared using the standard procedure starting with high-purity reagents such as titanium isopropoxide (TIPO), isoproponol and HNO_3. Ultra-cleaned glass slides were then dip-coated in this sol and kept overnight for drying at room temperature. The dried film was then heated at 60 °C, at which the films became porous. The thickness of the film was about 54 μm. in the next step the titania sol was hydrolyzed by adding it drop by drop to an appropriate quantity of distilled water under vigorous stirring. The whole volume was then heated to 60 °C for better crystallization of TiO_2 nanoparticles. Appropriate amount of tetraethyle orthosilicate (TEOS) was partially hydrolyzed in mixture of methanol, distilled water, dimethyleformamide (DMF), and HNO_3 by starring the solution for 30 min. To this partially hydrolyzed TEOS, required amount of TIOP was added and stirred for an hour. In this process, the mixing volume of the precursors was so maintained that the SiO_2/TiO_2 ratio becomes 95:5. Finally, dissolved Ho_2O_3 and yb_2O_3 in HNO_3 and stirred for an hour. In this particular molar concentration was added to it and the whole solution was stirred for another half an hour. The resulting sol was poured into small plastic molds for gelation at room temperature (22 °C). In this method, TiO_2 and SiO_2 interacted chemically, i.e., Ti-O-Si linkages were formed.

2.2 Characterization Techniques

The TGA/DTA of the prepared samples was done through a Perkin-Elmer (model: pyris Diamond). During TGA/DTA, the samples were heated from 40 °C to 800 °C at heating rate of 10 °C/min. The X-ray diffraction (XRD) of the sample was recorded using a Philip PW1710 X-ray diffractometer. The transmission electron microscopic (TEM) images were obtained through a using a JEM-2100 transmission electron microscope with recording voltage of 200KV. The optical absorption, Photoluminescence and up conversion spectra were measured at room temperature using iHR 320 imaging spectrometer (Horiba Jobin Yvon) with a 450 xenon (370 nm) and 980 nm diode laser.

3. Result and Discussion

3.1 TGA/DTA

The TGA/DTA studies were performed in order to determine the burn-off temperature of the templating agent, and also the final weight fraction of titanium dioxide. The TGA/DTA results are shown in Figure 1. An endothermic peak is observed at 89 °C in the DTA thermogram, which results from desorption of physically absorbed water and residual solvents. A large exothermic peak appears at around 211 °C, which is in the range of significant weight loss, as evident from the corresponding TGA. This exothermic peak can be attributed to the near complete combustion of organic compounds such as alkyl groups remaining in the solids. At approximately 275 °C, a small exothermic peak is observed, which can be assigned to the carbonization of remaining organic residues. TGA of the sample reveals that the weight loss below 127 °C is 13.35% and between 180 °C and 215 °C the weight loss is 50.16%. The weight loss could be attributed to the carbonization or the combustion of organic compounds.

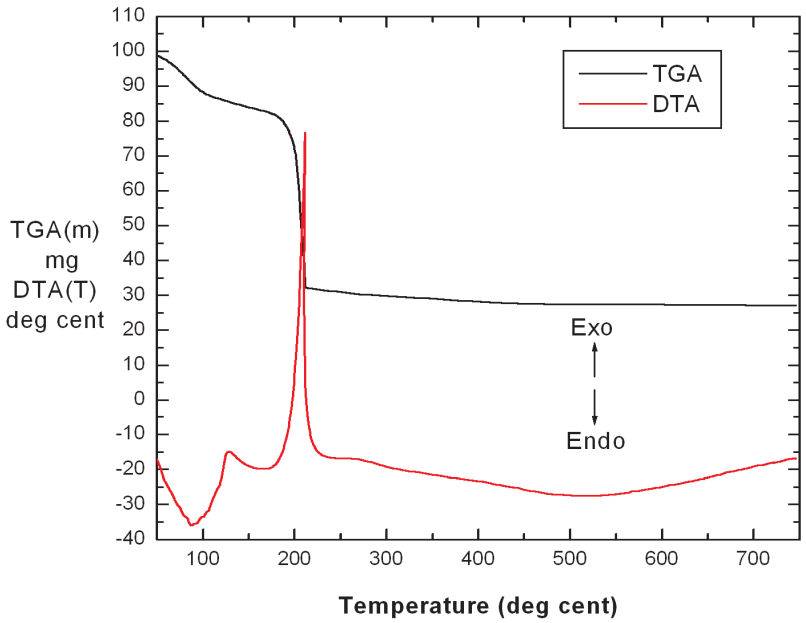

Figure 1. TGA/DTA of TiO_2-SiO_2

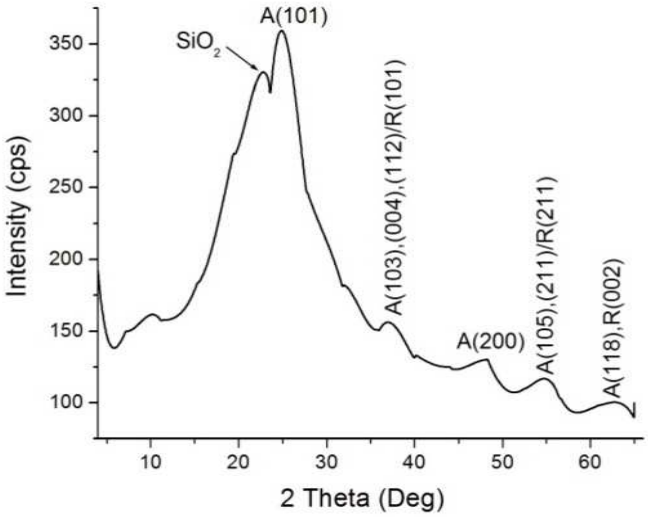

Figure 2. XRD of TiO_2-SiO_2

3.2 X-ray diffraction

The powder XRD patterns of the Ho^{3+} TiO_2-SiO_2 heated to 800 °C is shown in Figure 2. Two strong and relatively broad peaks can be seen at $2\theta = 6.246$ ° and 18.836 °, which can be assigned as due to Si_xO_2 ($0 < x < 1$). It is because of the fact that two peaks: one at $2\theta = 6.306$ ° and the other at $2\theta = 18.995$ ° have already been reported in the case of $Si_{0.98}O_2$ (JCPDS card no.: 81-2467). The small XRD peaks appearing at 25.499 ° and 54.013 ° indicate the presence anatase TiO_2 phases A (101) and A (105) respectively. The TiO_2 crystallite size calculated with the help of Debye-Scherrer formula, $t = 0.9\lambda/B\cos\theta$, where λ is the wavelength of x-ray radiation and B is the half with of the diffraction peak and θ is the angle. Using the anatase phase (101) peak of TiO_2 is 9.42 nm in diameter approximately.

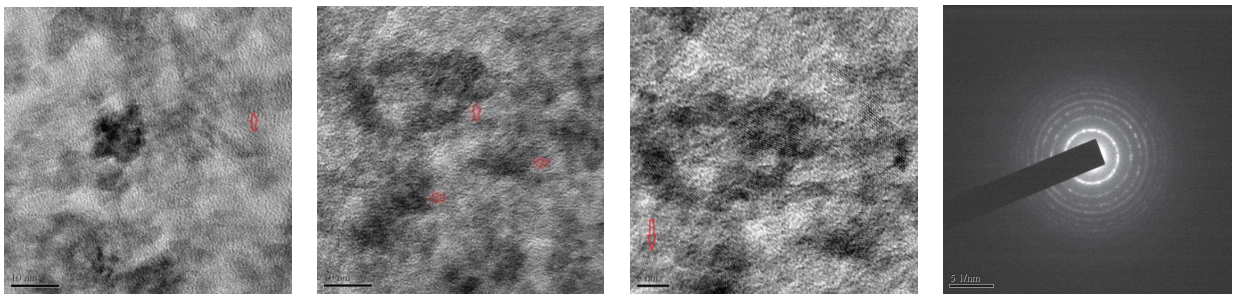

(a) (b) (c) (d)

Figure 3. TEM images, and the corresponding SAED pattern of (65 °C) nanocrystalline TiO_2 powder

3.3 TEM analysis of sol-gel prepared crystalline TiO_2 powder

For TEM investigation crystalline TiO_2 powders were the processing temperature in this case was 65 °C. The TEM images (at different magnifications) and the corresponding selected area electron diffraction (SAED) pattern of the TiO_2 samples are shown in Figure 3(a,b,c). Some oval (or spherical) and non-homogeneous structures can be easily seen in figures. The corresponding

SAED pattern (Figure 3(d) consists of sharp and aligned diffraction rings indicating that the TiO_2 nanoparticles are highly crystalline in nature [9]. It is seen that the lattice fringes over an entire oval-shaped TiO_2 particle (marked by an arrow) are uniform in nature. This, in turn, indicates that the individual particle consists of a single grain [9, 11]. Some TEM images of the same sample, at high resolutions, indicate the presence of particles within the size range of 7-10 nm in diameter. Thus, the TEM analysis has confirmed the possibility of existence of a 9.42 nm (in diameter)-sized TiO_2 crystallite as predicted by the XRD (using Scherrer formula). The corresponding SAED pattern Figure 3(d)) shows prominent Debye-Scherrer rings indicating that in this region, the TiO_2 nanoparticles in SiO_2 matrix are crystalline in nature. This indicates that some TiO_2 nanoparticles in the SiO_2 matrix consist of a single grain each, while some others are polycrystalline in nature.

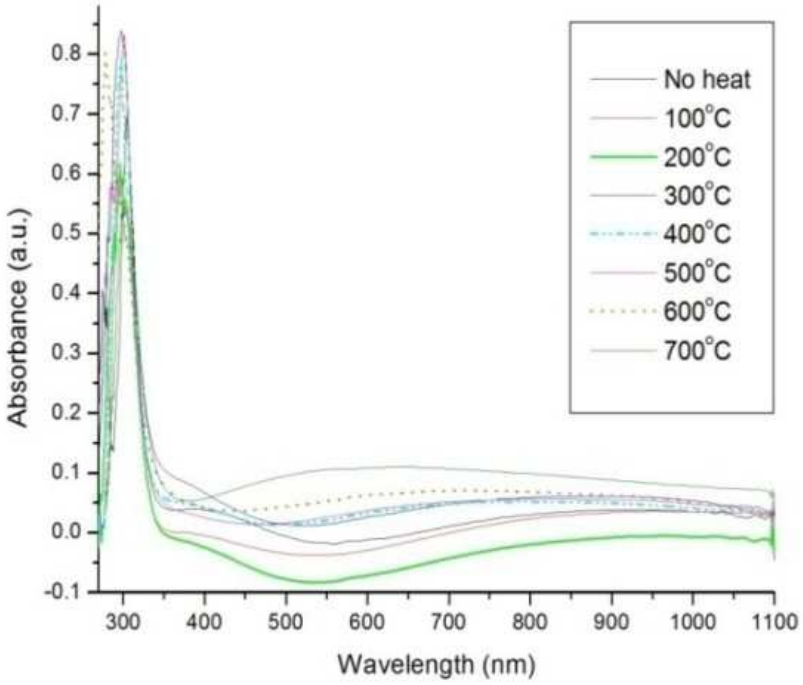

Figure 4. Absorption spectra of TiO_2 film at different temperatures

3.4 Absorption spectra of TiO_2 samples

The absorption spectra of an undoped TiO_2 film annealed at various temperatures are shown in Figure 4. The prepared films were highly transparent and they showed strong absorption in the ultraviolet (UV) region which is a characteristic of nano-sized TiO_2 particles. TiO_2 is an indirect band-gap semiconductor with band-gap energy (E_g) of about 3.1 eV for pure bulk anatase phase. The absorption edge for the TiO_2 film annealed at 200 °C lies near about at 330 nm. The corresponding energy of the absorption edge is about 3.761 eV, which is 0.661 eV higher than that of bulk anatase phase. This temperature is important, since the TiO_2 films showed a maximum "negative absorption" dip near 530 nm at 200 °C [6]. Just above to this absorption dip, there is a broad absorption band of the same film annealed at 700 °C.

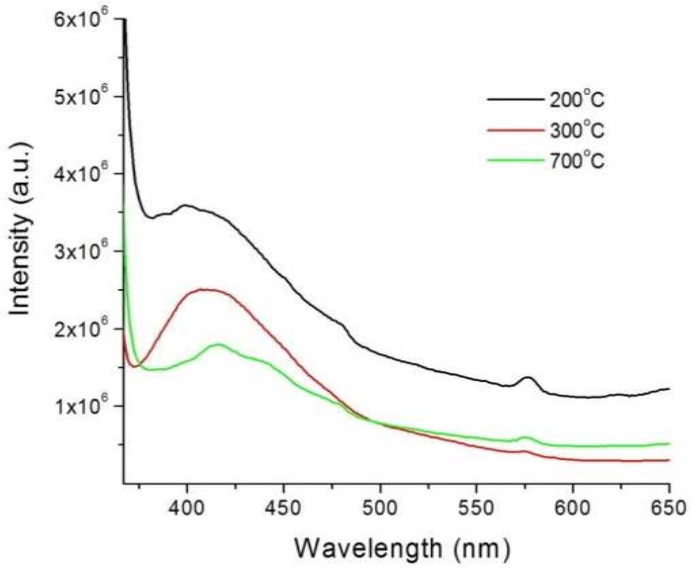

Figure 5. PL spectra of TiO_2 film

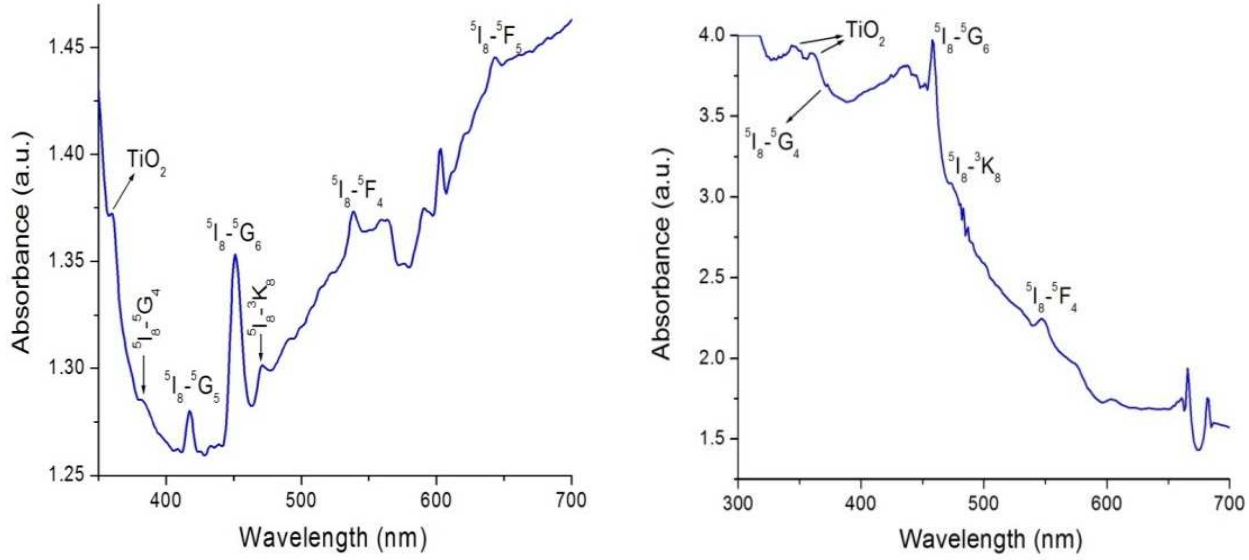

Figure 6. (a) Absorption spectra of Ho^{3+} 0.1 ml/20 ml TIPO, (b) Absorption spectra of Ho^{3+} 0.1 ml/20 ml TIPO

This 600 nm absorption band appears because of the formation of defects associated with oxygen vacancies that originate from the reduction of TiO_2 [6] after heat treatment at 700 °C. Here, the absorption edge of TiO_2 is at about 332 nm. The corresponding energy of the absorption edge is about 3.738 eV, which is 0.638 eV higher than that of bulk anatase TiO_2. The approximate particle size corresponding to the absorption edge can be estimated using the effective mass approximation (EMA) model [10] and is found to be less than 5 nm in diameter.

3.5 Photoluminescence emission and up conversion spectra of undoped TiO_2 film

The photoluminescence (PL) spectra of undoped TiO_2 film recorded under the excitations at 370 nm are shown in Figure 5 respectively. These spectra were taken for three different temperatures, 200 °C, 300 °C, and 700 °C.A broad peak around 400 nm is observed in the PL emission spectra of the TiO_2 film taken with 370 nm excitation. This 400 nm peak red-shifts with increase in heating temperature and corresponds to the direct recombination between electrons in the conduction band and holes in the valence band of TiO_2 [9]. The PL intensity is more in the case of the film annealed at 200 °C, the temperature at which the TiO_2 film showed a maximum "negative absorption" dip .

3.6 Absorption spectra of Ho^{3+} doped TiO_2-SiO_2

Absorption spectra of two 0.05 Ho^{3+}doped TiO_2-SiO_2 gel samples (heated at 65 °C) are shown in Figure 6(a). The sample thickness and refractive index are, 0.6 cm and 1.887. The concentration of TiO_2 precursor, i.e., titanium isopropoxide (TIPO) is 0.1 ml/20 ml of the sol from which the gel is formed. In the other sample Figure 6(b) the TIPO concentration is 0.5 ml/20 ml of the sol. The assignment of the peaks is shown in Table 1. It is seen that the number of distinct peaks of Ho^{3+} decreases with increase in TIPO concentration. The peak corresponding to the transition $^5I_5 \rightarrow {}^5G_5$ almost vanishes in the of (0.5 ml/20 ml) concentration of TIPO. Whereas it is prominent in the sample of 0.1 ml/20 ml of TIPO. The absorption bands near 345 and 360 nm can be assigned as due to TiO_2. The radiative transitions within the $4f^n$ configuration of a RE ion can be analyzed by the Judd-Ofelt (*J-O*) approach [14, 15]. The *J-O* theory gives an assessment of the oscillator strength characterizing the intensity of a transition between two $^{2S+1}L_J$ multiplets within the $4f^n$ configuration of a RE ion [6]. In the frame-work of the *J-O* theory, the theoretical oscillator strength (f_{cal}) is expressed as a sum of transition matrix elements involving the intensity parameters Ω_λ ($\lambda = 2,4,6$), which depends on the host matrix and is given by

$$f_{cal}(J,J') = \frac{8\pi^2 mc}{3h\lambda(2J+1)} \frac{(n^2+2)^2}{9n} \sum_{2,4,6} \Omega_\lambda \langle aSLJ\|U^\lambda\|a'S'L'J'\rangle^2, \tag{3.1}$$

where $(2J+1)$ is the multiplicity of the lower states, λ is the mean wavelength of the transition, c is the velocity of light in vacuum, m is mass of an electron, h is the Planck's constant and n is the measured refractive index. The transition matrix elements $\langle\|U^\lambda\|\rangle$ are essentially the same for different hosts. The experimental oscillator strength $f_{\exp}$ of the transitions were evaluated from integrating absorbance for each band and the relation is

$$f_{\exp} = 4.318 \times 10^{-9} \int \epsilon(\nu) d\nu, \tag{3.2}$$

where $\epsilon(\nu)$ is the molar extinction coefficient at wave number $\overline{\nu}$ cm^{-1}. The phenomenological intensity parameters Ω_λ for the forced electronic dipole transitions were obtained using MATLAB (MATLAB R12) commands at a suitable step of the calculation within the framework of the *J-O* theory. In this method, three adjacent and prominent peaks in the absorption

spectrum were taken. The reduced matrix elements were used in these calculations. The calculated Judd-Ofelt (*J-O*) intensity parameters Ω_λ are summarized in Table 1.

Table 1. Oscillator strengths and J O intensity parameters for HO^{3+}:TiO_2-SiO_2 glass

Transition	Energy (cm^{-1})	$f_{cal}(\times 10^{-6})$	$f_{cal}(10\times 10^{-6})$
$^5I_8 \rightarrow {}^5F_5$	15552	2.464	2.186
$^5I_8 \rightarrow {}^5F_4 + {}^5S_2$	18587	3.225	2.958
$^5I_8 \rightarrow {}^5F_3$	20619	0.808	0.931
$^5I_8 \rightarrow {}^5F_2 + {}^3K_8$	21131	0.331	1.172
$^5I_8 \rightarrow {}^5G_6$	22173	10.396	10.385
$^5I_8 \rightarrow {}^5G_5$	23981	1.793	1.999

$\Omega_2 = 1.972\times 10^{-20}\ cm^2$, $\Omega_4 = 1.469\times 10^{-20}\ cm^2$, $\Omega_6 = 1.227\times 10^{-20} cm^2$

The large value of Ω_2 indicate the presence of Ho-O-Ti covalent bond, since it is well established that that the parameter Ω_2 is structure sensitive and associated with the covalency and asymmetry of the RE ion in a particular host.

3.7 PL spectra of Ho doped TiO_2-SiO_2 nanocomposite gel

Figure 7 shows the PL spectra of Ho doped TiO_2-SiO_2 nanocomposite gel samples under 370 nm excitation the sample revealed strong emission bands near 434 nm, 461 nm and 490 nm (blue). The emission bands at green and red comparatively weak compared to blue bands are also observed at 547 nm and 620 nm In all the samples, the molar RE concentration was kept fixed while varying the TiO_2-precursor (TIPO) concentration. Some important radiative properties such as spontaneous emission probability (A_R), branching ratio (β_R) for different transitions and radiative life-time (τ_R) of excited states of Ho^{3+} in TiO_2-SiO_2 nanocomposite gels can be calculated using the value of *J-O* intensity parameters (Ω^λ).

$$A_R(\psi J;\psi' J') = \frac{64\pi v^3 e^2}{3hc^2(2J+1)}\left[\frac{n(n^2+2)^2}{9}S_{ed} + S_{nd}\right], \tag{3.3}$$

where S_{ed} and S_{nd} are electric and magnetic dipole line strengths respectively. The total radiative transition probability (A_R) of an excited state is given shown in Table 2.

Table 2. Calculated radiative parameters for Ho^{3+}:TiO_2-SiO_2 glass

Transition	Average energy	A_R	(β_R)	(τ_R)(μs)
$^5G_5 \rightarrow {}^5I_8$	23041	3265	0.482	147.60
$^5G_6 \rightarrow {}^5I_8$	21692	12883	0.860	66.76
$^5F_3 \rightarrow {}^5I_8$	20408	3321.71	0.816	257.07

In Table 2, the transitions $^5G_5 \rightarrow {}^5I_8$, $^5G_5 \rightarrow {}^5I_8$ and $^5F_3 \rightarrow {}^5I_8$ accounts for the largest values of radiative properties such as transition probability, branching ratio and life time in the excited state. It is concluded that the aforesaid transition of Ho^{3+} in TiO_2-SiO_2 glass has the potential to laser transition in the visible region.

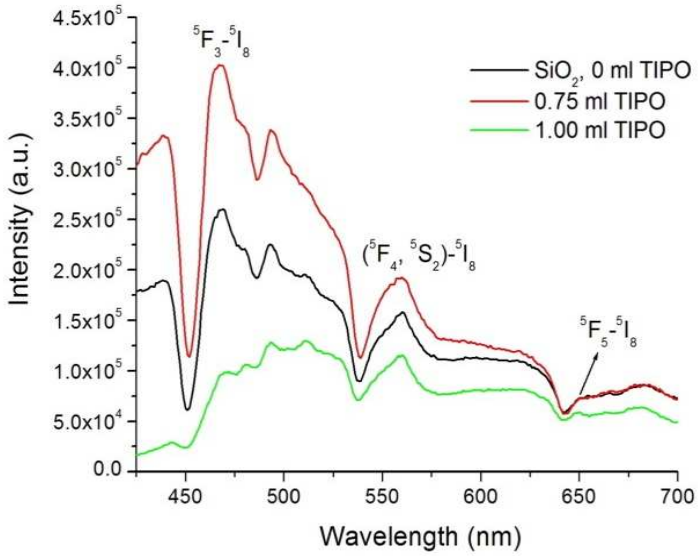

Figure 7. PL spectra of Ho^{3+} with different concentrations of TIPO

It is observed that the characteristics PL intensity of Ho^{3+} in silica xerogel initially increases as the TIPO concentration increases, reaches a maximum, PL intensity observed at 0.75 ml of TIPO. When the concentration of TIOP was further increased, we observed that the emission intensity declined. One possible explanation is that the TiO_2 particle act as network modifiers and increases the concentration of Si dangling and oxygen vacancy in the glass network. In this way, more electrons and holes can be easily excited and radiant recombination's and increased. Moreover, the interesting optical properties of the TiO_2 nanoparticles must be a significant factor. The presence of TiO_2 nanoparticles assist in the excitation of the RE ions by energy transfer from the TiO_2 particles to the RE ions. The decrease in PL with further increase in concentration may be due to the clustering of TiO_2.

3.8 Up Conversion Spectra

Up-conversion spectra of Yb^{3+}/Ho^{3+} is shown in Figure 8(a). It is seen that the up conversion intensity for the Ho^{3+}/Yb^{3+} doped SiO_2 glass sample made with 0.75 ml TIPO (per 20 ml) is much higher than that obtained for the Ho^{3+}/Yb^{3+}-doped SiO_2 glass (1.0 ml TIPO) (per 20 ml). So, TiO_2-SiO_2 systems can be much better host for RE ions than of simple SiO_2 glasses, provided a suitable RE concentration is used. The upconversion mechanism in Ho^{3+}/Yb^{3+} codoped TiO_2 nanoparticles under 980 nm diode laser excitation as described in Figure 8(b). The Yb^{3+} is initially excited from ground state $^2F_{7/2}$ to $^2F_{5/2}$ via absorbing a 980 nm photon and then transfers it to the Ho^{3+} ion in the ground state via ET process, thereby exciting it to the $^5I_6$ metastable state. Immediately following this process, subsequent ET from another Yb^{3+} ion

also in the excited state result in the population of the Ho^{3+} in $^5F_3$ and $^5F_4+^5S_2$ state from the metastable $^5I_6$ state through energy transfer (ET)and excited state absorption (ESA) and the excess energy is again dissipated by non radiative process. ESA process $^5I_6 \rightarrow ^5F_4+^5S_2$ absorption transition of Ho^{3+} is also possible because IR pumping phonon matches quite well with energy gap between the two states. Once the $^5F_3$ and $^5F_4+^5S_2$ states are populated, the major part of Ho^{3+} ions returns to the $^5I_8$ ground state. The band near 468 nm (blue) is assigned as due to the $^5F_3 \rightarrow ^5I_8$ optical transition. A distinct Stark-splitting is observed for this transition at 494 nm (blue). The emission band at 560 nm (green) corresponds to the ($^5F_4$, $^5S_2$) $\rightarrow ^5I_8$ transition. A relatively weak band centered on 650 nm (red) is also observed, which is due to the $^5F_5 \rightarrow ^5I_8$ transition. It is observed that the intensity of $^5F_3 \rightarrow ^5I_8$ is the highest among all the other transitions, which is usually not the case for the up conversion spectrum of Ho^{3+} observed in other reported glass host [12, 13]. Owing to the large absorption and emission cross section of Yb^{3+} ion is consider to be a preferable sensitizer for catching enough pumping energy and transferring considerable energy to Ho^{3+} ions in TiO_2-SiO_2 glass. The emissions are readily attributed to ET from yb^{3+} to Ho^{3+} ions. The UC intensity of Ho^{3+}/Yb^{3+} is approximately 2 times higher than the singly doped Ho^{3+} (not shown in figure) which confirmed that there exists an efficient energy transfer from yb^{3+} to Ho^{3+} ions.

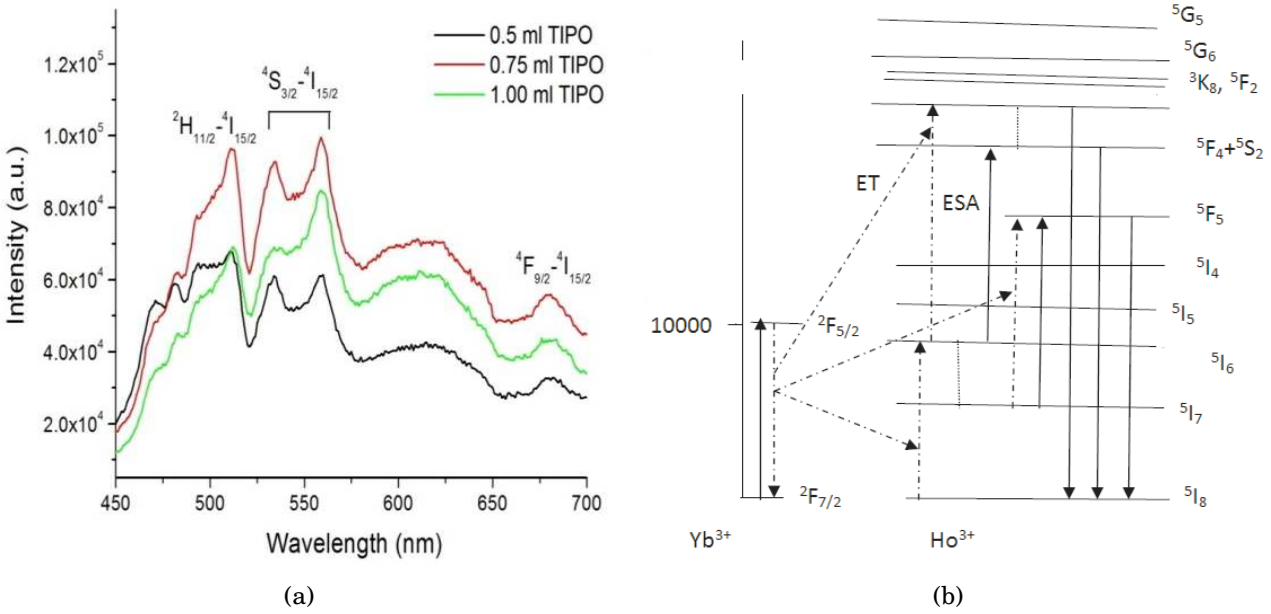

Figure 8. (a) UC spectra of Ho^{3+}/Yb^{3+} with different concentration of TIPO, (b) Energy level of Yb/Ho presented possible UC

4. Conclusions

The structural and optical properties of Ho^{3+} in TiO_2-SiO_2 were studied as a function of active ion concentration. The characteristics emission of Ho^{3+} was observed in the visible region. We observed the enhanced PL and UC of Ho^{3+} in TiO_2 nanoparticles embedded in SiO_2 amorphous matrices. By means of optical spectroscopy we observed that fluorescence of Ho^{3+} doped with

TiO_2 embedded in SiO_2 amorphous matrices was significantly dependent on concentration of TiO_2 nanoparticles. From the above result we deduce that TiO_2 nanoparticles enter the glass as a network modifier, increase the numbers of non-bridging oxygen in the glass network and weaken the Si-O bonds. This might be of interest for potential applications such as Laser amplifier and optical fiber communication and phosphor materials used in light emitting diodes.

Acknowledgements

The author is thankful to Department of Science and Technology, New Delhi for financial assistance (Project no: SR/S2/LOP-39/2010).

Competing Interests

The authors declare that he has no competing interests.

Authors' Contributions

Author wrote, read and approved the final manuscript.

References

[1] M.-J. Yoon, *Journal of Chinese Chemical Society* **56** (2009), 449–454.

[2] M. Abdel-Baki, F.A. Abdel-Wahab and F. El-Diasty, *J. Applied Physics* **111** (2012), 073506–073516.

[3] X. Wang, H. Lin, D. Yang, L. Lin and E.Y. Pun, *J. Applied Physics* **101** (2007), 113535–113542.

[4] J.W. Shi, J.T. Zheng and P. Wu, *J. Hazardous Materials* **161** (2009), 416–422.

[5] R. Reisfeld, *Materials Science* **20** (2002), 5–18.

[6] P.J. Dihingia and S. Rai, *J. Luminescence* **132** (2012), 1243–1251.

[7] F. Lahoz, I.R. Martin and J.M. Calvilla-Quintero, *Appl. Phy. Letter* **86** (2005), 51106–51108.

[8] I. Kamma and B. Rama Reddy, *J. Appl. Phys.* **107** (2010), 113102–11306.

[9] S.J. Kim, S.D. Park and Y.H. Jeong, *J. Am. Ceram.* **82** (1999), 927–932.

[10] Y. Kayanuma, *Phy. Rev. B* **38** (1988), 9797–9805.

[11] J.-L. Adman, *Chem. Rev.* **102** (2002), 2461–2476.

[12] A.A. Reddy, S.S. Babu, K. Pradeesh, C.J. Otton and G.V. Prakash, *Journal of Alloys and Compounds* **509** (2011), 4047–4052.

[13] P. Dutta and S. Rai, *Optik* **122** (2011), 858–863.

[14] B.R. Judd, *Phy. Rev.* **12** (1962), 750–761.

[15] G.S. Ofelt, *J. Chem. Phys.* **37** (1962), 511–520.